



Full length article

Critical assessment of hydrogen pipe diffusion at dislocations in metals

Xiao Zhou^{a,d,*}, Pengfei Ou^b, Normand Mousseau^c, Jun Song^{b,**}

^a State Key Lab of Metal Matrix Composites, School of Materials Science and Engineering, Shanghai Jiao Tong University, Shanghai 200240, China

^b Department of Mining and Materials Engineering, McGill University, Montréal, Québec H3A 0C5, Canada

^c Département de physique and Regroupement québécois sur les matériaux de pointe, Université de Montréal, Montréal, Québec H3C 3J7, Canada

^d Laboratory for Multiscale Mechanics Modeling (LAMMM), Institute of Mechanical Engineering, École Polytechnique Fédérale de Lausanne, Lausanne CH-1015, Switzerland

ARTICLE INFO

Keywords:

Hydrogen embrittlement
Hydrogen diffusion
Dislocation pipe diffusion
Atomistic simulations
Kinetic activation relaxation technique
Polyhedral structural unit

ABSTRACT

Hydrogen-dislocation interactions have always been a crucial problem in understanding and predicting the long-standing hydrogen embrittlement (HE) phenomenon in structural metals. Particularly with respect to hydrogen diffusion, dislocations have often been assumed with the ability to facilitate hydrogen transport via dislocation pipe diffusion (DPD). Yet the experimental and theoretical studies supporting DPD remain elusive and even controversial. In this work, hydrogen kinetics at dislocations in two representative metal systems, fcc Ni and bcc Fe, were systematically investigated combining comprehensive atomistic and kinetic activation relaxation technique simulations to reveal atomic details while enabling long-time (i.e., microsecond to second) hydrogen diffusion analysis. The dislocations were found to favor hydrogen trapping and provide regions of low migration barriers for hydrogen. However, these regions of low barriers only lead to localized fast short-circuit H diffusion, but do not translate into DPD over long time, which is attributed to fast hydrogen diffusion pathways along the dislocation line direction being periodically bound by high hydrogen migration barriers. Using the polyhedral structural units (PSUs) as an effective tool, we further quantitatively analyzed the correlation between hydrogen diffusion behaviors and local dislocation structures, illustrating the structural origin leading to local short-circuit diffusion and inhibition of DPD at dislocations. The new mechanistic insights gained not only are critical for understanding hydrogen-dislocation interaction, but also advances the general knowledge on hydrogen-microstructure interaction in structural metals.

1. Introduction

The interaction between hydrogen (H) and microstructures is of critical importance in understanding hydrogen embrittlement (HE), a phenomenon where H presence renders ductile metals and alloys prone to premature and brittle failure [1]. Microstructures provide interstitial sites of low-energy states to favor H segregation and accumulation [2–7], and at the same time, influence the kinetics of H [8]. One major aspect of H-microstructure interaction is the interplay between H and dislocations, the main microstructural entities responsible for plastic deformation in metals. Besides favoring H segregation, it has been suggested by many studies that dislocations can facilitate H transport [9–11]. In particular, it has been postulated by some researchers that dislocations offer low-barrier channels along their line directions to

enable fast H diffusion, namely dislocation pipe diffusion (DPD) [12]. DPD is often regarded as one mechanism responsible for enhanced H diffusivity in deformed metal samples [12–15]. The operation of DPD in facilitate H diffusion has been supported by nuclear magnetic resonance (NMR) [16] and quasielastic neutron scattering (QENS) [9] experiments that deduced lower activation barriers in the dislocation core or near-core regions. Meanwhile, there also exist simulation work such as the molecular static simulations by Tang et al. [11] and *ab-initio* calculations by Schiavone et al. [10], that show that there exist sites with low activation barriers for H migration in the partial cores in face centered cubic (fcc) Ni and Pd respectively.

In contrast to the afore-mentioned support for DPD, there have also been many studies questioning its occurrence in H diffusion [17–19]. Iwaoka et al. [20] performed electrochemical permeation tests on

* Corresponding author at: State Key Lab of Metal Matrix Composites, School of Materials Science and Engineering, Shanghai Jiao Tong University, Shanghai 200240, China.

** Corresponding author.

E-mail addresses: zhouxiao113@sjtu.edu.cn (X. Zhou), jun.song2@mcgill.ca (J. Song).

<https://doi.org/10.1016/j.actamat.2024.119758>

Received 8 November 2023; Received in revised form 10 February 2024; Accepted 12 February 2024

Available online 12 February 2024

1359-6454/© 2024 Acta Materialia Inc. Published by Elsevier Ltd. All rights reserved.

ultrafine-grained Pd to demonstrate that H diffusion is inhibited due to strong trapping by dislocations. Kimizuka et al. and Lu et al. carried out atomistic simulations on α -Fe and showed the absence of low-energy pathway for H diffusion along both screw and edge dislocation lines [18,21]. In addition, some recent studies for diffusion of interstitial carbon, being similar to H, at dislocation core structure via both atomic simulations and *ab-initio* calculation, suggest strong dependence of carbon diffusion behaviour on inherent geometrical features of dislocations [22,23] and a more complex relationship between diffusivity and DPD.

The conflicting options about DPD underline the current lack of clarity in the knowledge of interstitial impurity diffusion at dislocations, and call for further dedicated theoretical and simulation efforts to better our mechanistic understanding. Despite numerous simulation studies on DPD in structural metals [11,18,21–23], there exist several critical limitations in various simulation techniques employed. They are often focused only on a subset of H migration paths and H transition states, particularly for the case of *ab-initio* calculations where the simulation is confined in a very small system size, with timescale limited within nanosecond (e.g., in classical molecular dynamics (MD) simulations). Moreover, the previous simulations did not account for the influence of long-range elastic interactions on H kinetics. The limitations unavoidably cast shadow over the results or conclusions obtained. Consequently, it is necessary to re-investigate the problem with the afore-mentioned deficiencies addressed.

In the present work, we performed a comprehensive atomistic study of H kinetics at dislocations, encompassing not only mapping of activation barrier and energy landscape, but more important, the long-time (i.e., microsecond to second) diffusion behaviours, realized via the usage of kinetic activation relaxation technique (k-ART) [24–26]. Two representative metals of different crystal structure, namely face-centred cubic (fcc) Ni and body-centred cubic (bcc) Fe, were considered.

2. Computational methodology

For the two representative model systems considered in the present study, fcc Ni and bcc Fe, not only are they well-studied structural metals, but they also enable the consideration of dislocations in two different crystal structures. The two systems with H, denoted as Ni-H and Fe-H, respectively, are described by embedded-atom method (EAM) potentials [27,28] developed by Angelo et al. [29] and Ramasubramaniam et al. [30] respectively. Both potentials have been used in previous atomistic studies, and have been demonstrated to yield good descriptions of key physical properties and H-defect interactions [31–33].

For the Ni-H system, a rectangular simulation box with the crystal orientated as $x=[110]$, $y=[\bar{1}\bar{1}]$ and $z=[1\bar{1}\bar{2}]$ was constructed. A straight dislocation, being either edge or screw, was embedded in the center of the simulation box, as illustrated in Fig. 1a. Similar construction was done for the Fe-H system, with the crystal orientated as $x=[111]$, $y=[\bar{1}\bar{1}\bar{0}]$ and $z=[11\bar{2}]$ and enclosing a straight dislocation, as shown in Fig. 1b. The dislocation line, depending on whether it is edge or screw in nature, aligns with z or x direction respectively, being $[1\bar{1}\bar{2}]$ (edge) and $[110]$ (screw) in Ni, and $[11\bar{2}]$ (edge) and $[111]$ (screw) in Fe. The dislocation was introduced into the simulation box by displacing atoms according to the anisotropic elastic field, following the procedure outlined in [34]. The dimensions ($L_x \times L_y \times L_z$) of the simulation boxes containing an edge and screw dislocations are approximately $102 \times 121 \times 51 \text{ \AA}^3$ and $50 \times 122 \times 130 \text{ \AA}^3$ respectively for the Ni-H system, and $129 \times 113 \times 56 \text{ \AA}^3$ and $54 \times 121 \times 126 \text{ \AA}^3$ respectively for the Fe-H system. For all simulation boxes, periodic boundary conditions (PBC) were imposed on the dislocation line and slip directions while the free boundary condition was applied to the third direction.

After creation of the dislocation, molecular statics (MS) simulations were performed to examine the dislocation structure and H-dislocation

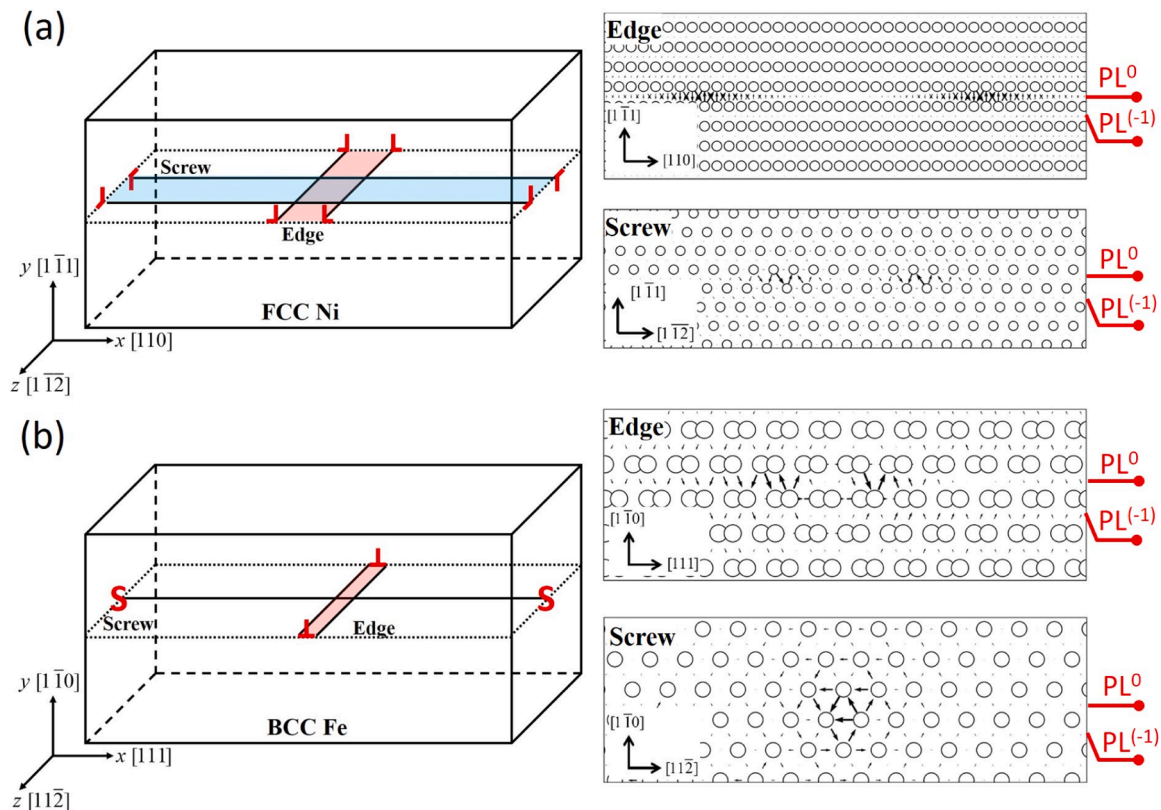


Fig. 1. Schematic illustration of the dislocation (edge or screw) containing simulation cells for (a) fcc Ni and (b) bcc Fe, where the edge and screw dislocation lines aligns with x and z directions respectively. The corresponding core structures with differential displacement mappings along the direction of Burger's vector are also shown. For simplicity, the glide plane and adjacent plane below are labelled PL^0 and $PL^{(-1)}$ respectively.

interaction. The system was then relaxed via energy minimization using the conjugate gradient (CG) method [35], implemented in the LAMMPS package [36]. The interstitial sites for H adsorption in the vicinity of a dislocation were identified [37], with their corresponding trapping states quantitatively assessed by the binding energy E_b , defined as:

$$E_b = E_{\perp}^H - E_{\perp}^0 - E_{bulk}^H + E_{bulk}^0 \quad (1)$$

where E_{\perp}^H and E_{\perp}^0 are the total energies of the dislocation containing system with and without an inserted H interstitial respectively, and E_{bulk}^H and E_{bulk}^0 denote the total energies of a perfect bulk lattice with and without an interstitial H atom respectively. In the above definition, positive and negative E_b values indicate endotherm and exotherm configurations respectively.

Meanwhile, nudged elastic band (NEB) calculations were performed to obtain the diffusion barrier of H around dislocation core regime. In parallel, on-the-fly kinetic Monte Carlo (KMC) simulations were also carried out over long time scale using kinetic Activation-Relaxation Technique (k-ART) so as to clarify H diffusion behaviours as a strong supplement for NEB calculations. k-ART is a powerful off-lattice KMC method with on-the-fly catalog building and an open-ended search technique for finding local transition states, being able to deal with complex lattice structures and account for long-range elastic interactions [27,38], which is completely deficient in NEB calculations. Furthermore, k-ART has the unique capability of simulating kinetics over long time scale (i.e., microsecond to second) beyond the otherwise nanosecond limit for atomistic simulations. It is also worth noting that all our k-ART simulations are performed at a fixed temperature of 300 K, since HE in structural metal frequently occurs in this temperature regime. Unbiased kinetic simulations are carried out by finding the H diffusion pathways and corresponding energy barriers in dislocations, so as to give us a clear kinetic picture of H in the regime of dislocations over long time.

3. Results and discussion

3.1. Mapping of H interstitials and energetics at dislocations

The relaxed dislocation core structures, along with the associated differential displacement maps are shown in Fig. 1. As noted in the figure, both edge and screw dislocations in Ni exhibit significant core splitting, with a sizable stacking fault between two partials. On the other hand, the dislocations in Fe show rather compact cores, with only slight core splitting at the edge dislocation while the so-called “easy core” with non-degeneration six-fold symmetry is observed for the screw dislocation, in agreement with previous studies [30]. It is clear from Fig. 1 that dislocations induce notable structural distortion in their close vicinity. Such distortion also necessarily affects the spatial arrangement of interstitial sites for H trapping, particularly them on the glide plane and the adjacent plane below, referred to as PL^0 and $PL^{(-1)}$ hereafter respectively, which is to be detailed below.

With the core structure obtained, the spatial distribution of interstitial sites in the vicinity of dislocation were then determined based on the identified polyhedral units [37,39], demonstrated in Fig. 2. For the Ni-H system, the dislocation, edge or screw, renders akin arrangements of interstitial sites for H on PL^0 and $PL^{(-1)}$ (c.f. Fig 2a-b) where these sites are octahedral units that exist in both near bulk lattice, dissociated partials and stacking fault regimes. For the Fe-H system, similar observations were found for the edge dislocation. However, the screw dislocation in Fe displays a much more compact core, and consequently, the core H interstitial sites exhibit a different spatial distribution and higher density than the bulk lattice (c.f., Fig. 2d). Besides affecting spatial distribution of H interstitial sites, dislocations have also strong effect on H binding energetics which is evidenced by the contour plots of H binding energies shown in Fig. 3. For the edge dislocation in Ni, the interstitial sites where H binding energies are notably affected, particularly the ones that favour H adsorption (namely trap sites for H), were found to mainly locate at PL^0 and $PL^{(-1)}$ planes, shown in Fig. 3a. The regions beneath the two partials on the $PL^{(-1)}$ plane were found to provide the most stable trapping sites, i.e., interstitial sites with the H binding energy around -0.18 eV. As for the screw dislocation in Ni, overall the H trapping capability is much weaker compared to the edge

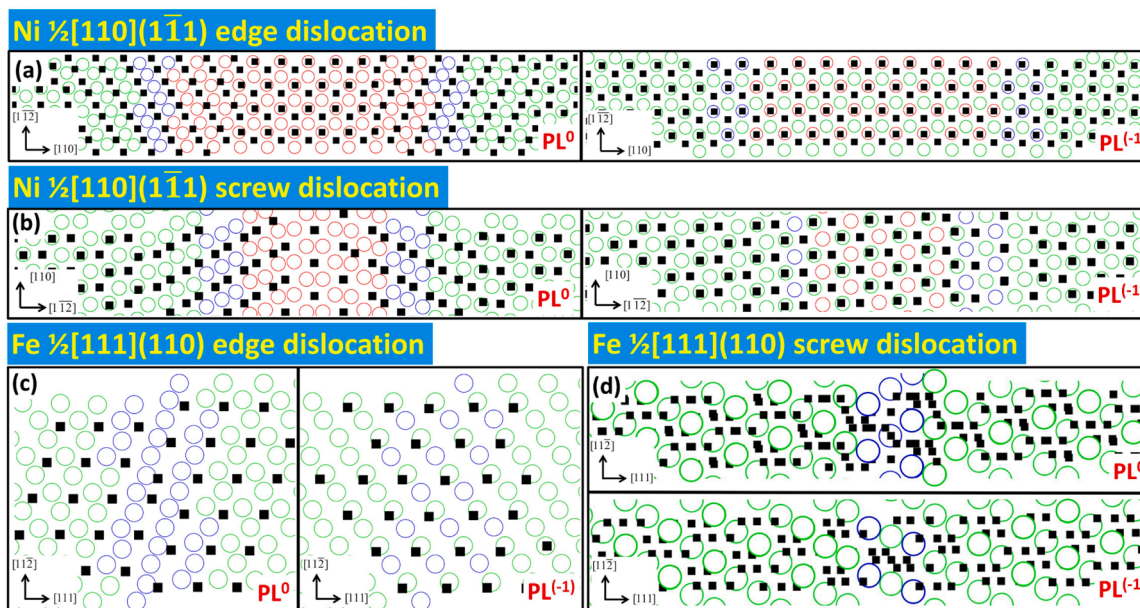


Fig. 2. Projected views of associated spatial locations of H interstitial sites in different planes (i.e., PL^0 and $PL^{(-1)}$, c.f. Fig. 1) at the vicinity of (a) edge and (b) screw dislocations in fcc Ni, and (c) edge and (d) screw dislocations in bcc Fe, with the projection direction being $[1\bar{1}1]$ and $[1\bar{1}0]$ for Ni and Fe respectively. The host atoms are indicated by large open circles where green, blue and red ones show atoms in bulk-like, dislocation core and stacking fault environments respectively, while H interstitial sites are indicated by small black solid squares.

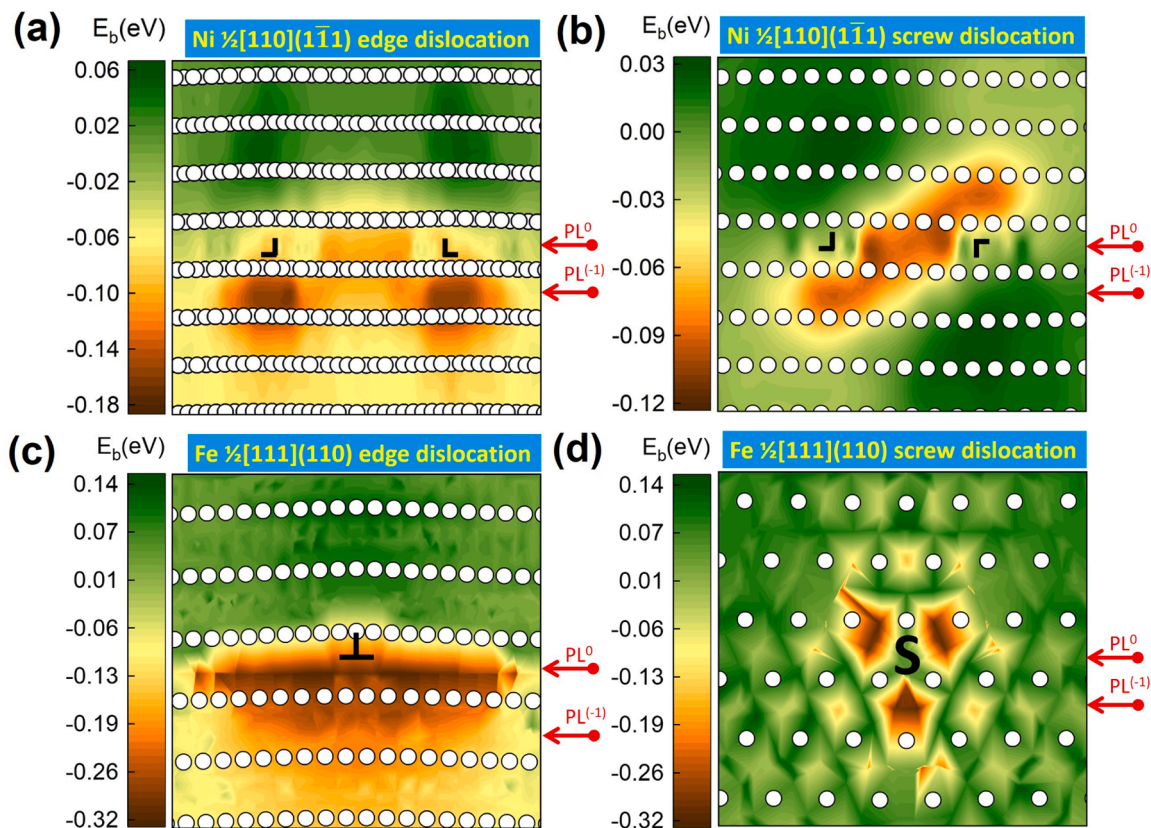


Fig. 3. The H binding energy contours at the (a) edge and (b) screw dislocations in fcc Ni, and (c) edge and (d) screw dislocations in bcc Fe. The white open circles represent the host metal atoms.

dislocation, which is well expected from the non-dilatational stress field. Nonetheless, the screw dislocation shows some weak trapping, as illustrated in Fig. 3b, where the most stable trapping sites are found on the PL^0 plane near the dislocation centreline, with a H binding energy about -0.1 eV. The above results for H energetics around dislocations in Ni are in good agreement with other work in the literature [11].

In the case of Fe, the H binding energy contours at the edge and screw dislocations are shown in Fig. 3c and Fig. 3d, respectively. Similar to the Ni case, much stronger trapping was observed at the edge than the screw. However, the contours show very different characteristics as seen when comparing Fig 3c-d with Fig 3a-b. For the edge dislocation in Fe, strong H trapping on both PL^0 and $PL^{(-1)}$ planes can be observed, but more concentrated around the dislocation due to little core splitting. Meanwhile for the screw dislocation, besides the similarly apparent low H trapping propensity, we note that the H binding energy contour exhibits a clear three-fold symmetry in Fe, which is again consistent with theoretical calculations by Kimizuka et al. in the literature [21].

3.2. Long-time H kinetics at dislocations

With the energetics of H at different dislocations characterized, the kinetics of H at dislocations was then investigated by k-ART over an extended time duration. As previously stated in the methodology section, all k-ART simulations were performed at room temperature (300 K). To facilitate reading, results are presented separately for Ni and Fe systems.

3.2.1. H at dislocations in Ni

Starting with the edge dislocation in Ni, we investigated various aspects of H diffusion using the k-ART simulations, with the results shown in Fig. 4. The k-ART calculated time evolution of the instantaneous H binding energy (E_b) is shown in Fig. 4a, from which the H

binding energy can be noted to span between -0.18 eV and 0.1 eV. This range is consistent with the H energetics mapping previously obtained by the MS simulations (c.f. $-0.18\sim 0.07$ eV). Fig. 4b shows the time evolution of the instantaneous energy barrier (E_m) of H migration at the edge dislocation, these barriers show a large fluctuation in value (between ~ 0 eV to 0.46 eV). This large fluctuation in E_m indicates that many different hopping events are occurring during H diffusion. Given that the energy barrier is ~ 0.4 eV for bulk H diffusion (denoted as E_m^0 hereafter), this also means that the dislocation presence can either facilitate and hinder H motion for those individual hopping events. It is also interesting to note from Fig. 4b that the E_m data are predominantly of values lower than 0.4 eV, indicating predominantly faster H (hopping) motions at the dislocation. Another observation from our k-ART results is that the motions of H are mostly occurring on the PL^0 plane. Though occasionally H was observed to hop to the adjacent planes, it would quickly jump back to PL^0 plane, as illustrated in Fig. 4d.

Comprehensive NEB calculations were also performed to supplement the k-ART simulations, and together the diffusion pathways and spatial distribution of H migration barrier E_m were obtained, shown in Fig. 5. We can see that the H diffusion pathways were substantially modified by the dislocation, being distinct from those in the bulk due to the drastic change of structural unit existed in the path. Examining the spatial mapping of E_m , we see that H migration exhibits low E_m in the partial core regions, while on the other hand, show high E_m in the center stacking fault region (0.54 eV) and at the boundaries with the bulk lattice (0.58 eV). It appears that the partial core regions could provide two channels of low E_m to potentially enable pipe diffusion of H. However, examining the time evolution of square displacement (SD) for H diffusion at the dislocation (c.f., Fig. 4c), we can observe a highly non-monotonic behavior. Though the SD exhibits quick increase over time for certain time periods (e.g., $25\sim 35\mu\text{s}$ and $190\sim 220\mu\text{s}$), it also shows sharp decrease over time for other time periods (e.g., $90\sim 150\mu\text{s}$),

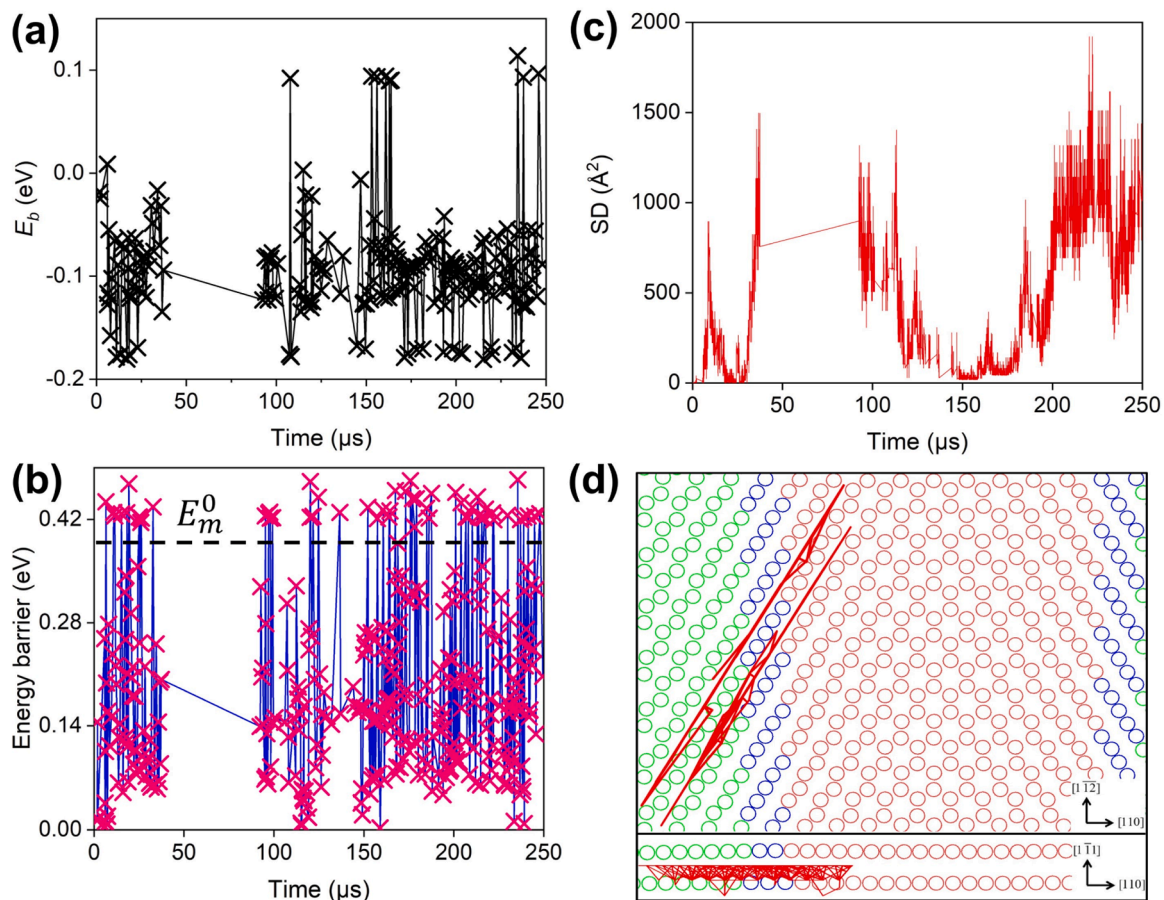


Fig. 4. Results at the $\frac{1}{2}[110](\bar{1}\bar{1}\bar{1})$ edge dislocation in fcc Ni, showing (a) binding energies vs. time evolution for H, (b) energy barrier vs. time evolution for H, where the black dash line represents the energy barrier (E_m^0) for bulk H diffusion, (c) the square displacement (SD) as a function of simulation time, and (d) projected and lateral views of H trajectories (marked by red lines) obtained by the k-ART simulations. The open circles are host atoms with green, blue and red ones indicating atoms in the bulk-like, dislocation core and stacking fault environments.

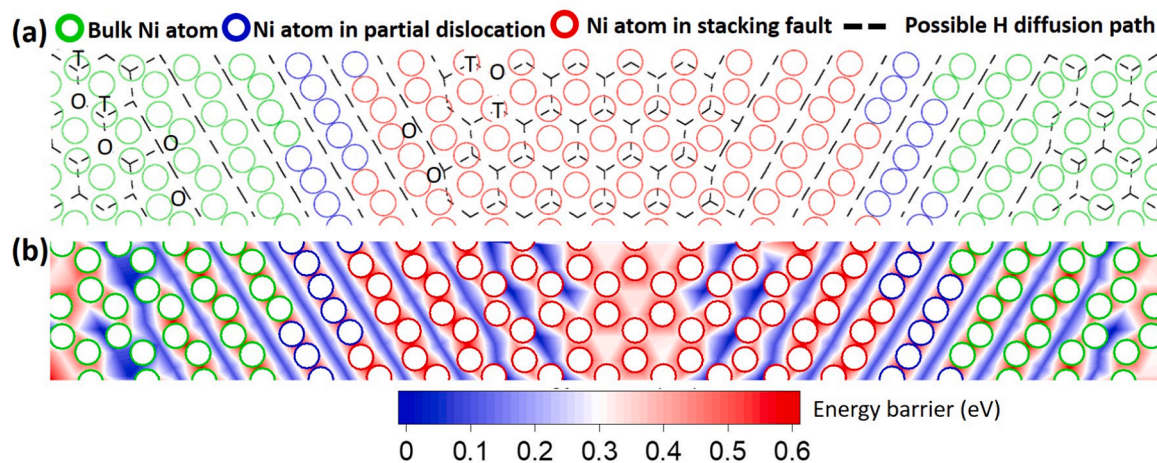


Fig. 5. (a) Possible H diffusion pathways on the glide plane, and (b) contour map of diffusion barriers, at the $\frac{1}{2}[110](\bar{1}\bar{1}\bar{1})$ Ni edge dislocation. In the figure, the octahedral and tetrahedral sites are representatively marked by “O” and “T” symbols respectively. In particular, tetrahedral sites are overlapped with host Ni atoms. Each hopping occurs between two neighbouring sites with dash line connection.

resulting in a ‘periodic’ fluctuation pattern. Longer k-ART simulations (up to $500\mu s$) were also performed to confirm the persistence of such fluctuation. Because of such fluctuation, we can see from Fig. 4c that overtime the SD for H diffusion at the dislocation will be far lower than that for H diffusion in the bulk. This indicates a much smaller effective H

diffusivity at the dislocation than bulk, and that the low-barrier channels in the partial core regions do not actually lead to fast H transport along the dislocation over time.

To understand the SD results shown in Fig. 4c, we examined the trajectory of H shown in Fig. 4d, where H can be seen to travel back and

forth along the low- E_m diffusion pathways within the partial core regions. As noted in Fig. 5, these pathways are not inclined to the dislocation line direction, thus H traveling along them would eventually get to the borders between the low- E_m partial core regions and their surrounding regions (i.e., either the stacking fault or bulk). However, the trajectory data demonstrate that H cannot easily cross those borders to escape, likely prevented by the high migration barriers bounding the partial core regions (c.f., Fig. 5b). That is, the high barriers, i.e., ~ 0.54 eV in the center stacking fault and ~ 0.58 eV at the boundaries with the bulk lattice, exhibit a blocking effect.

The effectiveness of observed blocking effect in PL^0 plane can also be examined by evaluating the detrapping timescale of H crossing those boundaries. The rate Γ of a special event leading to H crossing the boundary can be calculated as $\Gamma = \nu_0 \exp(-E_m/k_B T)$ where ν_0 is prefactor (10^{13} Hz), k_B is Boltzmann constant and T is temperature, and the inverse of Γ may be used as an estimate of the detrapping timescale. Plugging in the high barriers at the boundaries, i.e., 0.54 eV and 0.58 eV, we obtain Γ to be 2789 Hz and 377 Hz respectively, corresponding to detrapping time scales of 0.36 ms and 2.6 ms respectively. Both timescales are significantly greater than the timescale of H diffusion within the partial cores, indicative of long-time pipe diffusion being very difficult to occur. Consequently, H is effectively confined within the partial core regions, unable to move further along the dislocation line direction in PL^0 plane. This is in exact accordance with the SD results in Fig. 4c. The short-period quick increase/decrease in SD corresponds to fast H diffusion along the low- E_m diffusion pathways, while the periodic fluctuation corresponds to its constant reversal of diffusion directions due to the

inability to cross the boundaries to move further along. Thus, overall the results indicate that the edge dislocation in Ni, despite providing local regions of fast H motions, does not facilitate the global H transport along the dislocation, i.e., no occurrence of DPD.

Moving to the screw dislocation in Ni, the results from k-ART simulations are shown in Fig. 6. We note from Fig. 6a that H is sampling a binding energy range of -0.1 eV to -0.02 eV. The binding energies of H garnered during k-ART simulation are shown in Fig. 6a in which the binding energies are ranged from -0.1 to -0.02 eV, again consistent with the binding energy contour previously obtained from the MS calculations (c.f., Fig. 3b). Examining the migration barrier variation shown in Fig. 6b, we see that the E_m values are predominantly within 0.3 eV, much lower than the bulk E_m^0 of 0.42 eV, though occasionally high E_m (equal or exceeding E_m^0) events occur (e.g., 0.49 eV). Yet again the SD data (Fig. 6c) suggest that over time H transport is slowed than accelerated, and the trajectory data (Fig. 6d) show localized back-and-forth H motions within a confined region, despite the seemingly sizable reduction in the migration barriers of H motions by the dislocation as illustrated in Fig. 6b. Further examining the mapping of diffusion pathways and migration barriers are shown in Fig. 7, we see that, like the case of the edge dislocation in Ni, the screw dislocation also provides many low- E_m pathways in PL^0 plane. Yet again we notice that not only are these pathways inclined to dislocation line direction, they are also interrupted by high- E_m at places around the boundaries between partial cores and bulk lattices (~ 0.51 eV) as well as the central regime (~ 0.48 eV). Examining the H hopping events during k-ART simulations, the special events leading to H crossing the boundary exhibit detrapping timescales

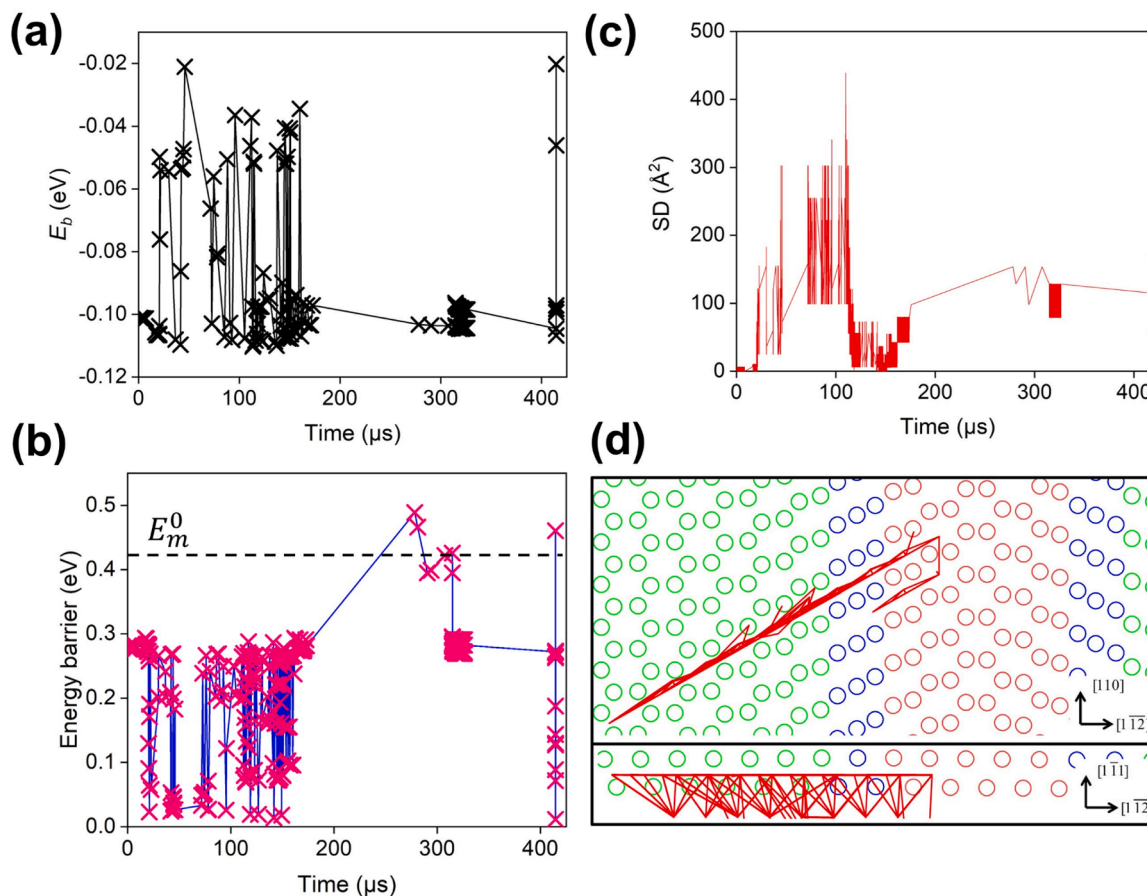


Fig. 6. Results at $\frac{1}{2}[110][\bar{1}\bar{1}1]$ screw dislocation in Ni, showing (a) binding energies vs time evolution for H, (b) energy barrier vs time evolution for H, where the black dash line represents the energy barrier (E_m^0) for bulk H diffusion, (c) the square displacement (SD) as a function of simulation time, and (d) projected and lateral views of H trajectories (marked by red lines) obtained by the k-ART simulations. The open circles are host atoms with green, blue and red ones indicating atoms in the bulk-like, dislocation core and stacking fault environments.

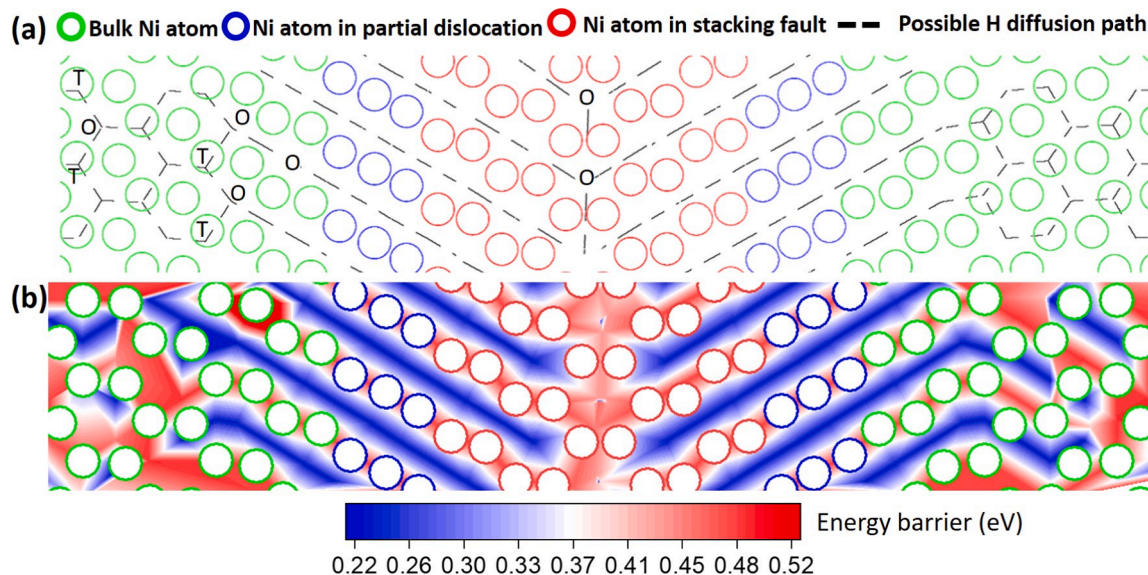


Fig. 7. (a) Possible H diffusion pathways in the glide plane, and (b) the contour map of diffusion barriers, at the $\frac{1}{2}[110](1\bar{1}1)$ Ni screw dislocation. In the figure, the octahedral and tetrahedral sites are representatively marked by “O” and “T” symbols respectively. In particular, tetrahedral sites are overlapped with host Ni atoms. Each hopping occurs between two neighbouring sites with dash line connection.

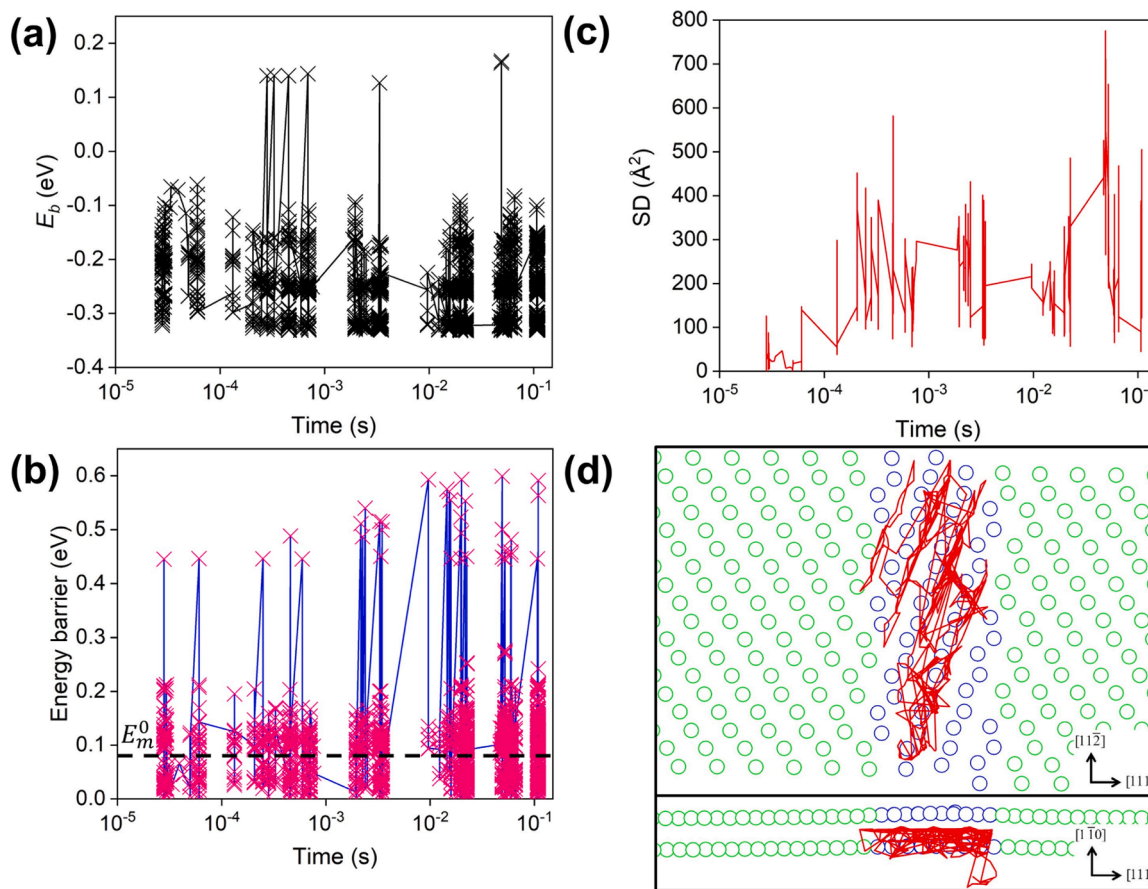


Fig. 8. Results at $\frac{1}{2}[111](110)$ edge dislocation in bcc Fe, with (a) binding energies vs time evolution for H, (b) Energy barrier vs time evolution for H, where the black dash line represents the energy barrier (E_m^0) for bulk H diffusion, (c) SD profile as a function of simulation time, and (d) projected and lateral views of H trajectories (marked by red lines) obtained by the k-ART simulations. The open circles are host atoms with green, blue and red ones indicating atoms in the bulk-like, dislocation core and stacking fault environments.

between 0.05 ms and 0.24 ms, three orders of magnitude higher than H diffusion in the core regions. Consequently, the high barriers bound the core regions prevent continuous H transport along the dislocation line direction and thus DPD. Moreover, again we can note from Fig. 6d that H activities are mostly within or at close vicinity to the PL^0 plane.

Our discussion above is focused on H diffusion in the PL^0 plane where H motions dominantly occur, as revealed by the k-ART simulations. However, in principle, H could detour to hop to the neighboring plane, e.g., the $PL^{(-1)}$ plane. Such detour also could enable H to avoid the blocking effects in the PL^0 plane. To this end, we examined such possibility. Yet, our results show that although H could hop to planes neighboring PL^0 , it does not in any way facilitate H diffusion or enable H to overcome the blocking effect. In addition, such cross-plane motion of H has a much higher forward barrier than the reverse one, and consequently H would always return to PL^0 shortly after it hops out. Consequently, practically H diffusion is always dominated by H activities within the PL^0 (see further details and discussion in the Supplementary Information).

To further quantitatively assess H diffusion, we employed the thermal statistic model [40,41] to calculate the diffusivity of H (D) at 300 K for edge and screw dislocation in fcc Ni (see more details in Supplementary Information), for diffusion on both PL^0 and $PL^{(-1)}$ planes. We noted that H diffusivities at dislocations are orders of magnitude smaller than the bulk value (see Fig. S6 in Supplementary Information). These results further confirm that dislocations do not enable fast diffusion, consistent with previous long-time k-ART simulations.

3.2.2. H at dislocations in bcc Fe

In the above we have demonstrated neither the edge or screw dislocation in fcc Ni can result in DPD despite their ability to reduce migration barriers for H motions locally. Instead, the presence of the dislocations renders long-range H diffusion more sluggish than the bulk lattice. For generality, below we investigate how H behaviors are influenced by dislocations in bcc Fe.

The k-ART results for the edge dislocation in Fe are shown in Fig. 8. From the aspect of H energetics, again we note the consistency in the H binding energy range of $-0.33\sim 0.14$ eV (c.f., Figs. 8a and 3) between the k-ART and MS simulations. From the aspect of kinetics, the k-ART results in Fig. 8b show that the migration barrier E_m of H hopping mostly oscillate in the range of $0\sim 0.22$ eV, while occasionally larger E_m values beyond 0.4 eV were observed. With the barrier of H diffusion in bulk Fe lattice being ~ 0.08 eV (i.e., E_m^0), the results indicate that the edge dislocation in bcc Fe has a dual effect on the migration barrier of H hopping.

Such dual effect of the edge dislocation on E_m is also well reflected in the NEB results shown in Fig. 9. Examining the spatial contour mapping

of E_m presented in Fig. 9b, first we can see that there exist low- E_m as well as high- E_m diffusion channels in the core region, being remarkably different from the bulk lattice diffusion. Second, we note that those low- E_m channels, where supposedly fast H transport can happen, are not interconnected, but separated from each other by high- E_m channels. Though the spatial mapping of E_m is different from those in the case of Ni, it again suggests that the long-range H transport along the dislocation line direction would be dependent on the ability of H overcoming high energy barriers from time to time. From the k-ART simulations, the hopping events that would enable H to cross from one low- E_m channel to another exhibit timescales between 0.08 ms and 1.8 ms, indicative of those events being heavily retarded. Now looking at the SD profile of H obtained from the k-ART simulations over long time duration (i.e., 0.1 s) shown in Fig. 9c, we can observe large fluctuation in SD, but without apparent increase of SD over time. This time evolution of SD indicates that those high- E_m channels effectively bar H from long-range transport, which is confirmed by the long-time trajectory of H around the edge dislocation shown in Fig. 8d. We can see from Fig. 8d that H are mostly confined to oscillate within the low- E_m channels and mostly within or at close vicinity to the PL^0 plane (see Fig. 8d), with limited sluggish motion along the dislocation line direction and no sign of DPD.

For the screw dislocation in bcc Fe, binding energies are found from both k-ART (see Figs. 10a) and MS (see 3d) simulations to range from -0.34 eV to -0.1 eV. Regarding H migration, the k-ART simulations showed that the E_m values for most H migration events were smaller than 0.13 eV while occasionally large E_m —beyond 0.2 eV—were observed, as shown in Fig. 10b. However, unlike those situations at dissociated dislocations (i.e., edge & screw dislocation in fcc Ni and edge dislocation in bcc Fe), H trapping at the screw dislocation in bcc Fe is confined to a small region due to the compact core. Such spatial confinement in H trapping was also found to be reflected in H kinetics, with H observed to mainly oscillate within the compact core, as shown by the H trajectories monitored (see Fig. S4 and the video S1/S2 in the Supplementary Information). Yet again H is found to be hardly able to escape from the core or travel along the dislocation line, as those motions correspond to hopping events of high migration barriers (confirmed by k-ART simulations). As a result, the overall low E_m locally rendered by the dislocation do not lead to no long-range H transport or DPD at screw dislocation in bcc Fe. Like the case of Ni, we have also examined H migration in neighboring planes to PL^0 and the cross-plane hops of H, and confirmed that both have little influence and do not alter H diffusion behaviors (see details in Supplementary Information). Also additional analysis on concentration dependent H diffusivity has been performed employing thermal statistic model [40,41] (see details in Supplementary Information).

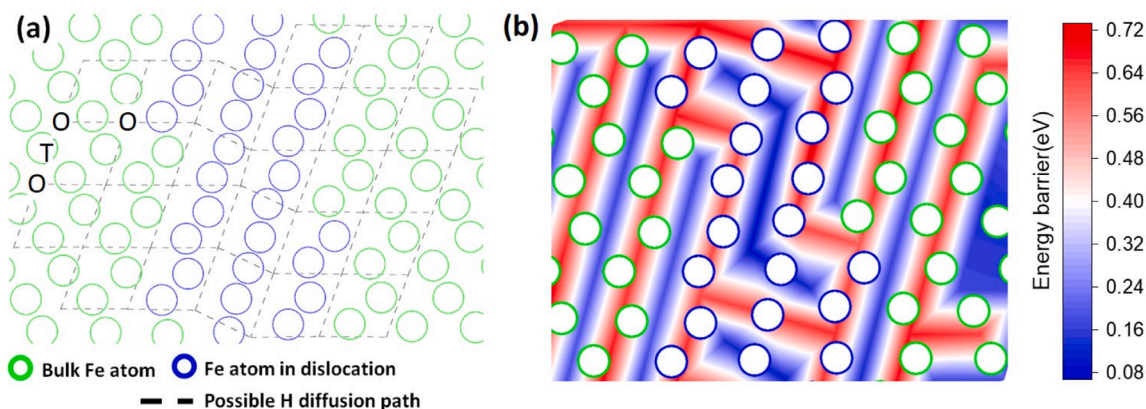


Fig. 9. (a) Possible H diffusion pathways in the glide plane, and (b) the contour map of diffusion barriers, at $\frac{1}{2}[111](110)$ edge dislocation in bcc Fe. In the figure, the octahedral and tetrahedral sites are representatively marked by “O” and “T” symbols respectively. In particular, tetrahedral sites are overlapped with host Fe atoms. Each hopping occurs between two neighbouring sites with dash line connection.

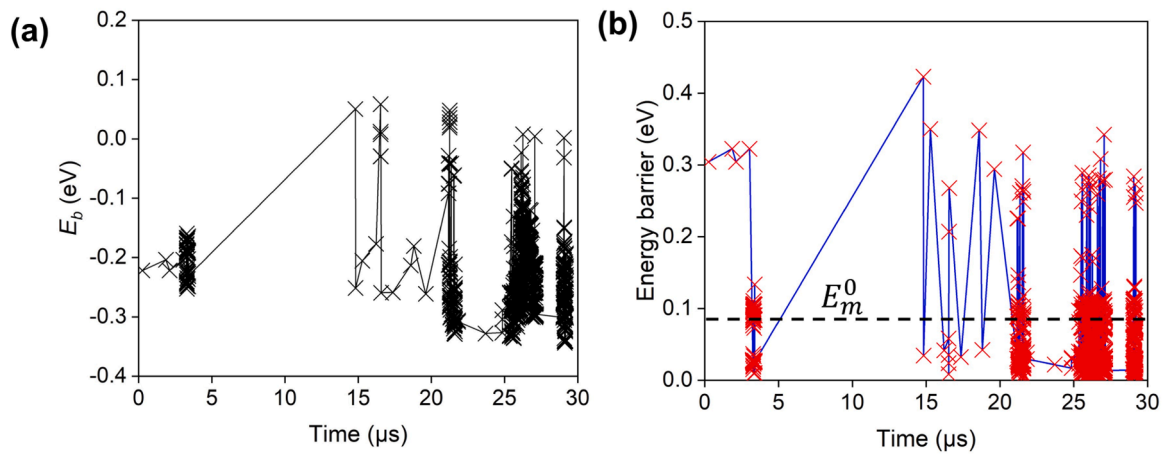


Fig. 10. (a) Binding energies vs time evolution for H, and (b) energy barrier vs time evolution for H, at $\frac{1}{2}[111](110)$ screw dislocation in bcc Fe.

3.3. Role of structural characteristics of dislocations on H kinetics

It is well recognized that the local diffusion behaviors of interstitials at microstructures, e.g., dislocations, are crucially affected or even prescribed by the structural characteristics, yet no quantitative linkage has been established despite many valuable attempts [22,23,33,42]. Our results above clearly show that the impact of dislocations on H kinetics is not a simple one and necessitates further analysis. In a previous study [37], we have demonstrated that the polyhedral structural units (PSUs) may serve as an effective tool for the description of geometrical features at microstructures, and are also structural units enclosing individual H interstitial sites. With dislocations represented in terms of PSUs, H diffusion is H traveling through a series of interconnected PSUs, which are effective “building blocks” constituting H diffusion pathways. Meanwhile, we may also quantitatively capture the local lattice distortion at dislocations through the geometrical change in PSUs, for which a simple geometrical change metric one can use is the PSU volume distortion, i.e., $\Delta V = (V - V_0)/V_0$ where V_0 and V are the volumes of a PSU in pristine lattice and at a dislocation respectively [37]. Positive and negative ΔV values indicate local lattice dilation and compression respectively. Fig. 11 shows the spatial mapping of ΔV of PL^0 plane for edge and screw dislocation in fcc Ni. Here we focus on ΔV for PL^0 plane as we have noted before that H motions are mostly within or at immediate vicinity to the PL^0 plane (c.f., Figs. 4d, 6d and 8d). Thus, the spatial mapping of ΔV is for PL^0 plane is expected to be most relevant to understand the kinetic activity of H.

As can be seen from Fig. 11, notably larger ΔV can be observed in the

vicinity of partial cores, while negligible ΔV is shown around bulk-like Ni region. Though the stacking fault region between two partial cores exhibits slightly higher ΔV values than the bulk, there is an abrupt drop in ΔV crossing from the core into the stacking fault. Comparing the ΔV mapping with the E_m mapping (c.f., Figs. 5 and 7) and H trajectory (c.f., Figs. 4 and 6), interesting correspondence can be observed. Fast H motions and dominantly H trajectory traces occur in the regions where PSUs are considerably and also consistently dilated. The locations where abrupt changes in ΔV occur nicely correspond to the places of significant E_m changes. Similar observation can also be made for the case of bcc Fe, for both edge and screw dislocations. Particularly for the screw dislocation in Fe, H exhibits a unique feature of PSU dilation along the dislocation line occurring in narrow and isolated strip regions, surrounded by regions of markedly negative ΔV . Such spatial distribution of PSU volume distortion is directly consistent with H kinetics and H trajectory profiles (see Fig. 12b, Fig. S5 and videos S1/S2 in the Supplementary Information). The above analysis and ΔV - E_m correspondence provides critical hints on the connection between H diffusion behaviors and local structural characteristics, demonstrating that the local volume distortion on base of the PSU concept may serve as one effective and qualitative tool for the quick diagnosis of H kinetics.

4. Conclusions

In summary, we have investigated systematically H kinetics at dislocations in two representative metal systems, fcc Ni and bcc Fe, combining comprehensive atomistic and k-ART simulations to reveal

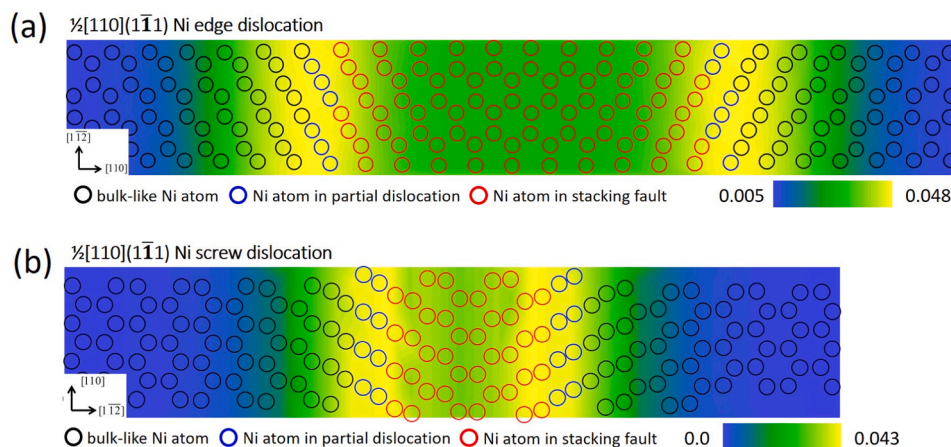


Fig. 11. Atomic configuration and the distribution of ΔV for PL^0 plane in (a) edge dislocation and (b) screw dislocations in fcc Ni.

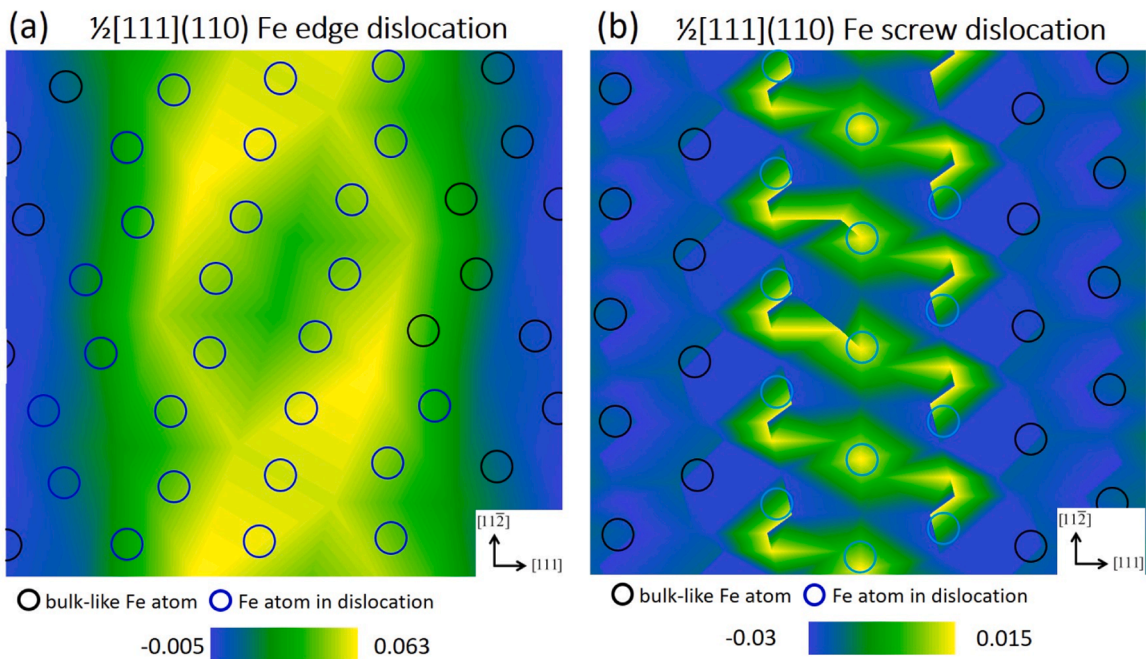


Fig. 12. Atomic configuration and the distribution of ΔV for (a) edge dislocation and (b) screw dislocation in bcc Fe.

atomic details while enabling long-time H diffusion analysis, with a focus to assess the possibility of dislocation *pipe* diffusion (DPD). The edge and screw dislocation cores examined in Ni and Fe, in general, are found to favor H trapping and to provide regions of low migration energies for H. However, these regions of low H migration energies may lead to localized fast short-circuit H diffusion, but do not translate into DPD. Rather, H transport along the dislocation line is considerably impeded. This can be attributed to fast H diffusion pathways along the dislocation line direction being periodically bound by high H migration barriers. These high barriers correspond to significantly larger H detrapping timescales than bulk H diffusion, and thus, effectively inhibit or even interrupt H transport along the dislocation line direction. An important take-away from the above results is that local fast motions of H does not necessary result in fast global H transport. We then demonstrated that the polyhedral structural units (PSUs) may serve as an effective tool to quantitatively analyze the correlation between H diffusion behaviors and local dislocation structures. In particular, the low-barrier regions where H motions are facilitated can be identified as places where PSUs experience consistent and continuous volume dilation. On the other hand, the high-barrier regions can be identified as locations where the volume distortion of PSUs undergoes drastic change. The PSU-based analysis is general and thus may be applied to other microstructural entities. Our findings provide a new perspective for critical assessment of DPD, and more broadly, the understanding of nanoscale H kinetics and transport behaviors at microstructures in structural metals.

Meanwhile, it is important to note that our present study is based on the simple edge and screw dislocation models. The dislocation structures in actual materials would be much more complex, with, e.g., mixed dislocations, dislocation junctions and even entanglement with other microstructure entities. In addition, the dislocations may also be subjected to the influence of stress. These complications could have profound impact on the operation of DPD and necessitate future studies. In addition, we would also like to caution about the inherent limitation of EAM potentials. Though they may be sufficient for the simple dislocation models, their validity in accurately describing complex dislocation structures and microstructures remains to be confirmed, an indispensable aspect to consider when we expand our investigation beyond the simple dislocation models, which necessitates dedicated future studies.

Declaration of competing interest

The authors declare that they have no known competing financial interests or personal relationships that could have appeared to influence the work reported in this paper.

Acknowledgement

X.Z. thanks National Key Research and Development Program of China (Grant No. 2022YFB3705701) and the National Natural Science Foundation of China (Grant No. 52301194) for financial support. X. Z., P. O., and J. S. thank the Natural Sciences and Engineering Research Council of Canada (NSERC) Discovery grant (grant RGPIN-2017-05187). N.M. acknowledges partial support from NSERC through a Discovery grant. We also would like to acknowledge Compute Canada for providing computing resources.

Supplementary materials

Supplementary material associated with this article can be found, in the online version, at [doi:10.1016/j.actamat.2024.119758](https://doi.org/10.1016/j.actamat.2024.119758).

References

- [1] W.H. Johnson, On some remarkable changes produced in iron and steel by the action of hydrogen and acids, *Proc. Royal Soc. Lond.* 23 (156–163) (1874) 168–179.
- [2] H. Rogers, Hydrogen Embrittlement of Metals: atomic hydrogen from a variety of sources reduces the ductility of many metals, *Science* (1979) 159 (3819) (1968) 1057–1064.
- [3] R.A. Oriani, Hydrogen Embrittlement of Steels, *Annu. Rev. Mater. Res.* 8 (1978) 30.
- [4] J.P. Hirth, Effects of hydrogen on the properties of iron and steel, *Metall. Trans. A* 11 (6) (1980) 861–890.
- [5] T. Tabata, H.K. Birnbaum, Direct observations of the effect of hydrogen on the behavior of dislocations in iron, *Scripta Metall.* 17 (7) (1983) 947–950.
- [6] M.I. Baskes, V. Vitek, Trapping of hydrogen and helium at grain boundaries in nickel: an atomistic study, *Metall. Trans. A* 16 (9) (1985) 1625–1631.
- [7] S.M. Myers, M. Baskes, H. Birnbaum, J.W. Corbett, G. DeLeo, S. Streicher, E. E. Haller, P. Jena, N.M. Johnson, R. Kirchheim, Hydrogen interactions with defects in crystalline solids, *Rev. Mod. Phys.* 64 (2) (1992) 559.
- [8] A. Turnbull, Perspectives on hydrogen uptake, diffusion and trapping, *Int. J. Hydrogen. Energy* 40 (47) (2015) 16961–16970.
- [9] B.J. Heuser, D.R. Trinkle, N. Jalarvo, J. Serio, E.J. Schiavone, E. Mamontov, M. Tyagi, Direct Measurement of Hydrogen Dislocation Pipe Diffusion in Deformed

- Polycrystalline Pd Using Quasielastic Neutron Scattering, *Phys. Rev. Lett.* 113 (2) (2014) 025504.
- [10] E.J. Schiavone, D.R. Trinkle, Ab initio modeling of quasielastic neutron scattering of hydrogen pipe diffusion in palladium, *Phys. Rev. B* 94 (5) (2016) 054114.
- [11] Y. Tang, J.A. El-Awady, Atomistic simulations of the interactions of hydrogen with dislocations in fcc metals, *Phys. Rev. B* 86 (17) (2012) 174102.
- [12] J. Tien, A.W. Thompson, I.M. Bernstein, R.J. Richards, Hydrogen transport by dislocations, *Metall. Trans. A* 7 (6) (1976) 821–829.
- [13] G. Itoh, K. Koyama, M. Kanno, Evidence for the transport of impurity hydrogen with gliding dislocations in aluminum, *Scr. Mater.* 35 (6) (1996) 695–698.
- [14] R. Kirchheim, J.P. Hirth, Interaction of hydrogen with dislocations in palladium—I. Activity and diffusivity and their phenomenological interpretation A2-Ashby, M.F. Perspectives in Hydrogen in Metals, Pergamon, 1986, pp. 355–363.
- [15] J. Albrecht, I.M. Bernstein, A.W. Thompson, Evidence for dislocation transport of hydrogen in aluminum, *Metall. Trans. A* 13 (5) (1982) 811–820.
- [16] A. Boukraa, G. Styles, E. Seymour, A 2D NMR study of deuterium trapping by dislocations in palladium, *J. Phys. Condens. Matter* 3 (14) (1991) 2391.
- [17] D. Bombac, I. Katzarov, D. Pashov, A. Paxton, Theoretical evaluation of the role of crystal defects on local equilibrium and effective diffusivity of hydrogen in iron, *Mater. Sci. Technol.* 33 (13) (2017) 1505–1514.
- [18] T. Lu, Y.P. Xu, X.D. Pan, H.S. Zhou, F. Ding, Z. Yang, G.J. Niu, G.N. Luo, X.C. Li, F. Gao, Atomistic study of hydrogen behavior around dislocations in α iron, *J. Nucl. Mater.* 510 (2018) 219–228.
- [19] H. Ogawa, Atomistic simulation of hydrogen dynamics near dislocations in vanadium hydrides, *J. Alloys. Compd.* 645 (2015) S205–S208.
- [20] H. Iwaoka, M. Arita, Z. Horita, Hydrogen diffusion in ultrafine-grained palladium: roles of dislocations and grain boundaries, *Acta Mater.* 107 (2016) 168–177.
- [21] H. Kimizuka, S. Ogata, Slow diffusion of hydrogen at a screw dislocation core in α -iron, *Phys. Rev. B* 84 (2) (2011) 024116.
- [22] A. Ishii, J. Li, S. Ogata, Conjugate channeling” effect in dislocation core diffusion: carbon transport in dislocated BCC iron, *PLoS. One* 8 (4) (2013) e60586.
- [23] R. Xie, S. Lu, W. Li, Y. Tian, L. Vitos, Dissociated dislocation-mediated carbon transport and diffusion in austenitic iron, *Acta Mater.* 191 (2020) 43–50.
- [24] G.T. Barkema, N. Mousseau, Event-based relaxation of continuous disordered systems, *Phys. Rev. Lett.* 77 (21) (1996) 4358–4361.
- [25] N. Mousseau, G.T. Barkema, Traveling through potential energy landscapes of disordered materials: the activation-relaxation technique, *Phys. Rev. E* 57 (2) (1998) 2419–2424.
- [26] F. El-Mellouhi, N. Mousseau, L.J. Lewis, Kinetic activation-relaxation technique: an off-lattice self-learning kinetic Monte Carlo algorithm, *Phys. Rev. B* 78 (15) (2008) 153202.
- [27] M.S. Daw, M.I. Baskes, Embedded-atom method: derivation and application to impurities, surfaces, and other defects in metals, *Phys. Rev. B* 29 (12) (1984) 6443.
- [28] R. Johnson, Alloy models with the embedded-atom method, *Phys. Rev. B* 39 (17) (1989) 12554.
- [29] J.E. Angelo, N.R. Moody, M.I. Baskes, Trapping of hydrogen to lattice defects in nickel, *Model. Simul. Mat. Sci. Eng.* 3 (3) (1995) 289.
- [30] A. Ramasubramaniam, M. Itakura, E.A. Carter, Interatomic potentials for hydrogen in α -iron based on density functional theory, *Phys. Rev. B* 79 (17) (2009) 174101.
- [31] J. Von Pezold, L. Lymperakis, J. Neugebauer, Hydrogen-enhanced local plasticity at dilute bulk H concentrations: the role of H–H interactions and the formation of local hydrides, *Acta Mater.* 59 (8) (2011) 2969–2980.
- [32] M. Itakura, H. Kaburaki, M. Yamaguchi, T. Okita, The effect of hydrogen atoms on the screw dislocation mobility in bcc iron: a first-principles study, *Acta Mater.* 61 (18) (2013) 6857–6867.
- [33] Y. Zhao, G. Lu, QM/MM study of dislocation—Hydrogen/helium interactions in α -Fe, *Model. Simul. Mat. Sci. Eng.* 19 (6) (2011) 065004.
- [34] P.M. Anderson, J.P. Hirth, J. Lothe, *Theory of Dislocations*, Cambridge University Press 2017.
- [35] J.W. Daniel, The conjugate gradient method for linear and nonlinear operator equations, *SIAM. J. Numer. Anal.* 4 (1) (1967) 10–26.
- [36] S. Plimpton, Fast parallel algorithms for short-range molecular dynamics, *J. Comput. Phys.* 117 (1) (1995) 1–19.
- [37] X. Zhou, D. Marchand, D.L. McDowell, T. Zhu, J. Song, Chemomechanical origin of hydrogen trapping at grain boundaries in fcc metals, *Phys. Rev. Lett.* 116 (7) (2016) 075502.
- [38] M. Trochet, L.K. Béland, J.F. Joly, P. Brommer, N. Mousseau, Diffusion of point defects in crystalline silicon using the kinetic activation-relaxation technique method, *Phys. Rev. B* 91 (22) (2015) 224106.
- [39] S. Huang, D. Chen, J. Song, D.L. McDowell, T. Zhu, Hydrogen embrittlement of grain boundaries in nickel: an atomistic study, *npj, Comput. Mater.* 3 (1) (2017) 28.
- [40] Y.A. Du, J. Rogal, R. Drautz, Diffusion of hydrogen within idealized grains of bcc Fe: a kinetic Monte Carlo study, *Phys. Rev. B* 86 (17) (2012) 174110.
- [41] X. Zhou, N. Mousseau, J. Song, Is hydrogen diffusion along grain boundaries fast or slow? atomistic origin and mechanistic modeling, *Phys. Rev. Lett.* 122 (21) (2019) 215501.
- [42] Y. Zhao, L. Dezerald, J. Marian, Electronic structure calculations of oxygen atom transport energetics in the presence of screw dislocations in tungsten, *Metals. (Basel)* 9 (2) (2019) 252.